Journal of Thermal Analysis and Calorimetry (2023) 148:12059–12070
https://doi.org/10.1007/s10973-023-12520-7

Microfluidics temperature compensation and tracking for drug injection based on mechanically pulsating heat exchanger

G. C. Sankad[1] · G. Durga Priyadarsini[2] · Magda Abd El-Rahman[3] · M. R. Gorji[4] · Nizar Abdallah Alsufi[5]

Received: 22 February 2023 / Accepted: 20 August 2023 / Published online: 13 September 2023

Abstract

To assure correct patient care and lower pharmaceutical mistakes that might cause serious harm or death, this research introduces a microfluidic heating flowmeter for tracking injectable pumping based on a mechanically pulsating heat exchanger. It is impossible to use the usual gravimetric approach for flow-rate measurement in clinics because it necessitates extensive preparations and laboratory equipment. Consequently, there is a huge need for a standard technique substitute that can be used for distant, frequent, small-scale infusion-pump surveillance. Here, to give precise measurements, the research presents a downsized heated flowmeter made of a silicon platform, a platinum heating layer atop a silicon dioxide thin membrane, and polymer microchannels. A microfluidics temperature compensation and tracking method is suggested in this research. Based on this architecture, the research put forth a heat transmission concept in which the researchers looked at the regional correlations among the macro-scale temperature detector and the microscale liquids. The accuracy of temperature management for microscale reagents was demonstrated using a series of temperature-sensitive nucleic acid multiplication experiments. The efficacy of the heat transport model is further confirmed by comparisons of mathematical and empirical data. The isothermal multiplication polymerase chain reaction temperature-related minor fluctuations in fluorescence intensity could be identified with the aid of the compensatory method that was given. If the amplifying temperature differs by 1 °C, the likelihood density plots of fluorescence intensity are significantly different from one another. This technique is useful for micro–macro-interaction monitoring generally and extends beyond microfluidic purposes.

Keywords Microfluidics · Temperature monitor · Mechanically pulsating heat exchanger · Temperature compensation

✉ G. C. Sankad
math.gurunath@bldeacet.ac.in

M. R. Gorji
mohammad.rahimigorji@ugent.be; m69.rahimi@yahoo.com

Nizar Abdallah Alsufi
na.alsufi@qu.edu.sa

[1] Department of Mathematics, B.L.D.E.A's V. P. Dr P. G. Halkatti College of Engineering and Technology, Vijayapur, Karnataka 586103, India

[2] Department of Mathematics, Geethanjali College of Engineering and Technology, Cheeryal, Hyderabad, Telangana 501301, India

[3] Department of Physics, College of Science, King Khalid University, 61413 Abha, Saudi Arabia

[4] Faculty of Medicine and Health Sciences, Ghent University, 9000 Ghent, Belgium

[5] Department of Management Information System and Production Management, College of Business and Economics, Qassim University, P.O. BOX 6666, 51452 Buraydah, Saudi Arabia

Introduction to microfluidics and temperature monitoring

One of the pieces of medical gear that clinics utilize the most frequently is an infusion pump. Mechanically pulsating heat exchanger infuses medicinal liquids into a patient's circulation scheme in regulated amounts and at exactly predetermined rates, such as nutrition, medicines, and contrast agents [1]. Pump malfunctions can result in overdose, missing therapies, or disruption in therapy because of the nature of the fluids they are designed to deliver, particularly high-risk drugs. This has a substantial impact on the wellness and security of the sufferers. From 2005 to 2009, the US Food and Drug Regulation recorded around 56,000 incidents of unfavourable infusion pump-related events, including several injuries and fatalities [2]. The infusion pump's inefficiency when operated improperly is the cause of one of its most well-known failures. While the infusing pump's clinical instructions call for correctness with a 5% maximum

margin of error, current precision personalized medicine and treatment need tightly regulated medicines administered on schedule. Drug injections for new born babies, and young children, for instance, must be able to administer several doses of high quantities at slow fluid velocity [3]. Since supplying the low-volume liquid needs more accurate fluidic management than providing the huge volume, this medicinal requirement is a considerable issue in the smaller end (3.0 g h^{-1}).To maintain patient security, a flow-rate sensor that can calibrate the infusing pump within the low region is essential [4].

The gravimetric model (GM) is the foundation of the infusing pump's standardized calibrating process. The quantity of the injectable liquid is measured by the GM using a balance, and the mass increase multiplied by ignition timing is used to compute a traceable flow velocity (in the unit of g h^{-1}). To prevent any miscalibration caused by fluid drifting, vaporization, and bubbling, accurate GM needs precisely regulated equipment, such as draft screens, microtubing, and dispensed syringes [5]. Due to these limitations, the GM is normally carried out in a carefully regulated laboratory setting and cannot be implemented in hospitals, homecare settings, outlying medical institutions, or while providing care while travelling. There is a high need for an alternative to the GM that is ideal for these infrequent, small-scale, and distance adjustments of the infusing pump. The development of downsized flowmeter platforms has proven to benefit from microelectromechanical system (MEMS) technologies [6]. Optical, mechanical, and heating flowmeters are some of the MEMS measurements that have been studied thus far. The most popular of them are the heat flowmeters, which are made up of just a few components (such as metallic warmers and temperature monitoring) and are simpler and more sensitive than non-thermal flowmeters.

Direct connection and non-direct connection thermometer monitoring are the two primary approaches that have been documented for microfluidics temperature monitoring [7]. In general, the temperatures can be precisely measured, but contact assessment will change the natural temperatures of the intended microfluids through external macro-equipment [8]. Because there is no heat transfer when using non-contact measuring equipment, it is challenging to attain high precision by relying on variations in the targeted object's physical characteristics.

To apply indirect ways to flip the microfluidic temperatures, more and more microscopic heat exchange concepts have been discovered and examined in recent times. The impact of heat transmission from the pipe substance is not taken into account when, for instance, copper wire is wound across a microfluidic pipe to serve as a temperature shift resistor to detect microfluidic temperatures. Temperature-sensitive materials that turn green can be used to detect microfluidic thermal variations, but they typically work best at a single temperature and have a relatively limited range of uses. The use of liquid metals with low breaking temperatures as easy-to-handle compounds with excellent thermal conductance in microfluidic heat exchange has also received much study [9]. To obtain a ratio of thermal transmission, fluid metals can be utilized as heating conductive mediums to link the microscopic and the macroscopic worlds. The electromagnetic flowmeter is made up of an electrically insulated fibre pipe. Electrodes positioned opposite the additional, magnetic coil installed on pipe to generate magnetic field, and further forth. The insulated pipe transports the liquid, the flow that has to be monitored. A temperature monitoring system maintains and controls the temperature of a certain environment. In recent years, temperature monitoring systems have become a vital component of health care, hospitals, clinics, the food industry, and other businesses.

In a heat exchanger, conduction and convection operate in concert to transfer heat. Heat exchangers can feature four different flow configurations: cross flow, co-current or parallel flow, and hybrid flow. Regenerative and recuperative heat exchangers are neither of the primary kinds of heat exchangers.

The research offers a MEMS flowmeter that combines a microfluidic channel with a small membrane and a heating element to provide a quick reaction time, a low level of ambiguity, and minimal power consumption using a mechanically pulsating heat exchanger. The efficiency of the gadget was assessed using GM as a benchmark [10]. The flowmeter's dimensions are 11.5 mm × 17.5 mm × 3 mm, making it suited for a variety of liquid-flow calibrating applications in the field. This study presents a unique indirect temperature measuring technique that integrates a fluid metallic sensor with a millimetre-scale platinum impedance commercial sensor to detect and track the temperatures of microfluidic chip channels. This approach is user-friendly, reproducible, and avoids direct contact between the detector and the microfluid. A measure to offset and compensate an unfavourable temperature affect is referred to as temperature compensation. A sensor's measured value should never again be impacted by a temperature change thanks to temperature compensation. The mechanical varieties of water flowmeters, which measure flow by turbine rotation with a propeller, shunt, or paddle wheel design, are the most popular and cost-effective kind of water flowmeter. Glass-based microfluidic devices have emerged as a game-changer in the field of microfluidics because of its many advantages over silicon, MFTCTM, and paper in terms of photonics, electronics, and thermochemistry.

The remainder of the research is organized in the following manner. Section 2 indicates the background to the temperature measurement in microfluidics. The proposed microfluidics temperature compensation and tracking method (MFTCTM) is designed and analysed in Sect. 3. Section 4

illustrates the simulation analysis and the findings of the study. The conclusion and the findings of the research are shown in Sect. 5.

Background to the temperature measurement in microfluidics

Including sample collection, processing, and storing, sample processing, signal conversion and enhancement, mechanical sensing, and power providing, well-designed microfluidic systems may achieve great multiple functionalities in wearable technology. Furthermore, wearable microfluidic gadgets have shown potential uses in clinical evaluation, monitoring of wellness, and communication between intelligent gadgets and people. This study primarily concentrates on the general functionalities and architectures of multipurpose wearable technology based on microfluidic gadgets, as well as their specific implementations in physiological signal surveillance, clinical diagnostics and treatments, and health care [11].

The research created a microfluidic device with high-precision platinum (Pt) thermo-sensor integrated that can cultivate cells and track the temperatures of the cells in real time [12]. A fixed temperature system with 0.015 °C of reliability was used during the detection process. The Pt thermo-temperature sensor's coefficients of impedance were 2090 ppm/°C, giving it a temperature precision of less than 0.008 °C. As a result, the thermogravimetric microchip combined with tissue culture may be a non-disposable and label-free instrument for tracking cellular temperatures used in the research of physiology and disease.

To examine algal development under various culture settings, the research offers gradient-based microfluidic devices [13]. Using the gadget, it gives the chance to create droplets with various medium nutrient availability in 200 s, saving the time and reagent from having to prepare these solutions the traditional way. The system is regarded as the third attempt to use a gradient chip in the field of algae biotechnology. It is exceptional, easy to use, and produces very competent outcomes.

The research created a portable microfluidic device that combines repressor polymerase multiplication (RPM) with a person's body heat for an easy and quick multiplication of HIV-1 DNA [14]. In the ambient setting, the normal body temperatures at the wrist ranged between 33 and 34 °C, which is suitable for RPM responses. This device consistently identified HIV-1 DNA in the range of 102 to 105 copies mL^{-1} with a log predictability of 0.98 in 24 min using a cell phone-based fluorescent detection approach. These findings show that in terms of speed, mobility, and electricity autonomy, this wearing point-of-care (POC) nucleic acid monitoring approach outperforms conventional PCR and alternative isothermal polymerase chain reaction techniques.

This study discusses a variety of microfluidic techniques, including culturing and tracking adhering and non-adherent cells, as well as several microfluidic device characteristics [15]. The paper compares the systems that are now accessible with high-throughput research, automation capabilities, interface to devices, and connectivity. Factors, such as the operating adaptability of the gadgets, are assessed in terms of their diagnostic effectiveness. Advanced microfluidics' ability to perform multiple functions has led to the discovery that a significant amount of scientific results can be obtained from a single system, enabling complex innovative power and effective data correlation—both of which are crucial when considering biomedical research.

For temperature control in microfluidic devices, the research provides a modular, adaptable, and self-sufficient convection heat transfer [16]. The heat transfer is made of polymeric tubes that are totally immersed in elastomer blocks and wound around with a polymer pole to be installed into the microfluidic chip with ease. It works with a variety of microfluidic substrates and geometries. To move the heat-carrying fluid through heat transfer at the necessary fluid velocity and heat, miniature, battery-powered vibrating pumps are used.

The research describes a sensor device to track the oxygen intake by mammalian cells as a direct signal for metabolism while taking the needs for utilization in Biolabs into account [17]. This entails accurate oxygen sensing, a compact configuration devoid of complex external apparatus, the use of appropriate components, and the capacity to achieve a high level of connectivity and robotics. A system that comprises heaters, a temperature probe, external optical reading, a hydrodynamic chip with an embedded oxygen-sensitive phosphors layer, 3D-printed supports, and an enclosure satisfies these criteria.

To achieve accurate and quick temperature management in the region between 2 and 37 °C, a combined microfluidic gadget with active components for cooling and warming was designed [18]. The system, which was made up of a desiccator, a microheater, and a temperature probe, managed to change the local heat on the chip actively through responses. The linked modelling of heat transmission, flow properties, and heat conduction involved multiphysics simulations. The design parameters for achieving precise and rapid control of on-chip local thermal control were confirmed by the simulation and modelling methods.

The production of materials with nano- or microscale dimensions has been a research priority for many years, and the development of microfluidic techniques offers alternate methods for doing so [19]. The latest events in the manufacture of nano-microsized nanoparticles with specified characteristics employing various Microfluidics

(MDs), including continuously laminar flow, segmented stream, droplet-based, and other non-chip centred microreactors, are discussed, along with their biological implications.

Quick halide transfer of inorganic polycrystalline nanocrystals is described in a simple room-temperature method [20]. Using a flexible microfluidic technology called the quantum dot exchanger, the research isolates reaction percentage from precursor mixing rates to offer a thorough knowledge of the halide transfer processes. On the pace and scope of the halide exchange processes, the impacts of ligand content and the origin of the halogen salt are demonstrated.

Omar Abu Arqub et al. (2014) detailed to enable to efficiently solve systems of second-order boundary value problems that work introduces the continuous genetic algorithm (GA), which relies on smooth solution curves throughout its evolutionary process in order to get the necessary nodal values of the unknown variables [21]. Nodal values provided by genetic operators are used to transform the challenge of solving the system of differential equations into one of minimizing the global residue or optimizing the fitness function. In degree to solve systems of second-order boundary value problems, the suggested approach is shown to be a reliable and precise technique by the numerical results.

Zaer Abo-Hammour et al. (2014) introduced the optimization approach, the continuous genetic algorithm, for numerically approximating the solutions to Troesch's and Bratu's problems [22]. To begin with, it should not need more complex mathematical tools; that is, the algorithm should be easy to comprehend and apply and therefore readily accepted in the mathematical and physical application sectors. Second, in terms of the answers found and its capacity to handle other mathematical and physical issues, the algorithm is of global character. Third, the suggested approach has an implied parallel aspect, implying that it would be implemented on parallel computers.

Emad H. M. Zahran et al. (2023) examined the major goal of this research was to generate a large number of novel forms of soliton solutions for the Radhakrishnan-Kundu-Lakshmanan equation, which depicts unstable optical solitons that originate from optical propagations using birefringent fibres [23]. These novel forms were discovered using four separate techniques: the extended simple equation method, the Paul-Painlevé approach method, the Ricatti–Bernoulli-sub ODE method, and the solitary wave ansatz method. The novel solitons can be assembled to produce a soliton catalog with new amazing characteristics and can contribute to future research not just for this model but also for optical propagations via birefringent fibre.

According to the analysis of the literature, microfluidics research has temperature measurements. However, many lack short of expectations of performance and precision. In an effort to facilitate drug injection, a better method is created to account for and monitor the temperatures in microfluidics.

Proposed microfluidics temperature compensation and tracking method

This section deals with the working principle, material selection process, fabrication process, thermal flowmeter characterization setup for analysis, and parameters for numerical analysis are discussed in this section.

Working principle and design

Steady power and steady temperatures are the two separate sensing methods used by the current flowmeter. The heating temperature is measured using the continuous power (CP) method, while the heating power is kept constant. The amount of liquid or gas that passes through a pipeline in a certain amount of time is measured by a flowmeter. Flowmeters, measuring flow rates, provide essential insight into material is flowing across pipes, drainage systems, and other forms of infrastructure. Due to the increasing heat exchange, the heating temperature drops as the flow rate rises. Equation (1) shows a description of a one-dimensional concept of the heating temperatures.

$$T_{\mathrm{h}} = \frac{h_{\mathrm{p}}}{k_{\mathrm{t}} w_{\mathrm{h}} \left(\frac{l_{\mathrm{t}}}{\propto} + \sqrt{4k + \frac{v\sigma^2}{4b^2}} \right)} \tag{1}$$

where T_{h} denotes the temperature of the heating element, h_{p} denotes the heat output, k_{t} denotes the heat capacity of the liquid, w_{h} denotes the heater's thickness, l_{t} denotes its length, $\propto$ denotes the width of the boundary surface, v denotes the average flow rate, b denotes the fluid's diffusion coefficient, and k denotes the incompressible component, the thermoelectric undertake Even though the heater's impedance changes a little bit according to the flow speed, it is safe to presume that the overall power stays constant. The right-hand side of Eq. (1) is therefore constant, except v, $\sqrt{v}$ has an inverse relationship with T_{h}.

In continuous temperature (CT) mode, the exterior electrical circuit modifies the current to maintain a consistent resistance (heat) of the heat source [21]. To account for heat transfer and sustain the temperatures, the warming power must rise as the flow rate does. Equation (1) is used to represent a one-dimensional model of heat load, where T_{h} is steady and P is proportionate to $\sqrt{v}$. The little membrane that surrounds the heater reduces the k component, lowering the amount of P and T_{h} needed to retain responsiveness. Additionally, the tiny heat capability has

the benefit of shortening the time it takes to attain a steady state, producing a quick response time.

The design and working process of the flowmeter is denoted in Fig. 1. The basic architecture is shown in Fig. 1a, and the substrate view is shown in Fig. 1b, respectively. A platinum (Pt) covering with warmers and poles, a polydimethylsiloxane (PDMS) channels layer, and silicon substrates with a silicate dioxide/silicon nitrogen (SiO_2/SiN_x) membrane make up the flowrate. Each radiator is situated on the $800 \times 800 \times 0.8$ mm silicone SiO_2/SiN_x membranes. Due to its great sensibility for flow monitoring, the membranes only permit the transmission of heat to the liquid and not to the substrates. To have a rapid reaction period and great responsiveness, membranes that are smaller and wider are preferable. To reduce heat circulation through the platform and increase heat convection via the liquid, the researchers chose a membrane width of 0.8 mm, which is more than 500 times narrower than the silicon substrates. Additionally, this concept's ultralow thermal capability allows for a substantial reduction in the reaction period. The research created films that were 600 µm, 800 µm, and 1000 µm broad to find the ideal membrane thickness (data not shown). The research discovered that an 800-µm-wide membrane was the best flowmeter foundation because a 1000-µm-wide membrane had poor manufacturing yield and inconsistent physical endurance during the flow assessment.

This configuration can complement the stress concentration (compressive pressure for the SiO_2 and compressive strength pressure for the SiN_x) for the robust physical features and flat morphological attributes of the tissue. The structure of the membrane phase included 150-nm-thick SiN_x wedged by 300-nm- and 350-nm-thick SiO_2 tiers. A mechanically pulsating heat exchanger on either side acts as a benchmark sensor for fluid temperature measurement upstream and downstream. To function in constant energy or fixed temperature mode, the burner in the centre acts as a flow-sensing component. The heater is made up of serpentine electrical wiring with a width of 10 pm and a total dimension of 0.19 mm by 0.20 mm. The heating may function as both a warmer and a temperature probe since it is linked to four electrical wires for 4-wire remotely sensed. The PDMS channel has a width of 0.5 mm or 1.5 mm and a height of 100 µm. The 0.5-mm-wide thin stream was chosen because it would completely cover the heating surface with 190 µm width. Then, to study the impact of bandwidth, a 1.5 mm wide channel was selected, making it three times broader than the narrow strait [22]. Due to the simplicity of production while utilizing SU-8 2050, 0.1 mm for the channel height was ultimately chosen. A critical design consideration, too-low fluid flow lowers flowmeter accuracy and a 0.1 mm canal height demonstrated a velocity distribution of at least 10 mm h^{-1} at a 0.5 g h^{-1} flow rate. The microchannel has inlet/outlet apertures on both sides and is 10 mm long

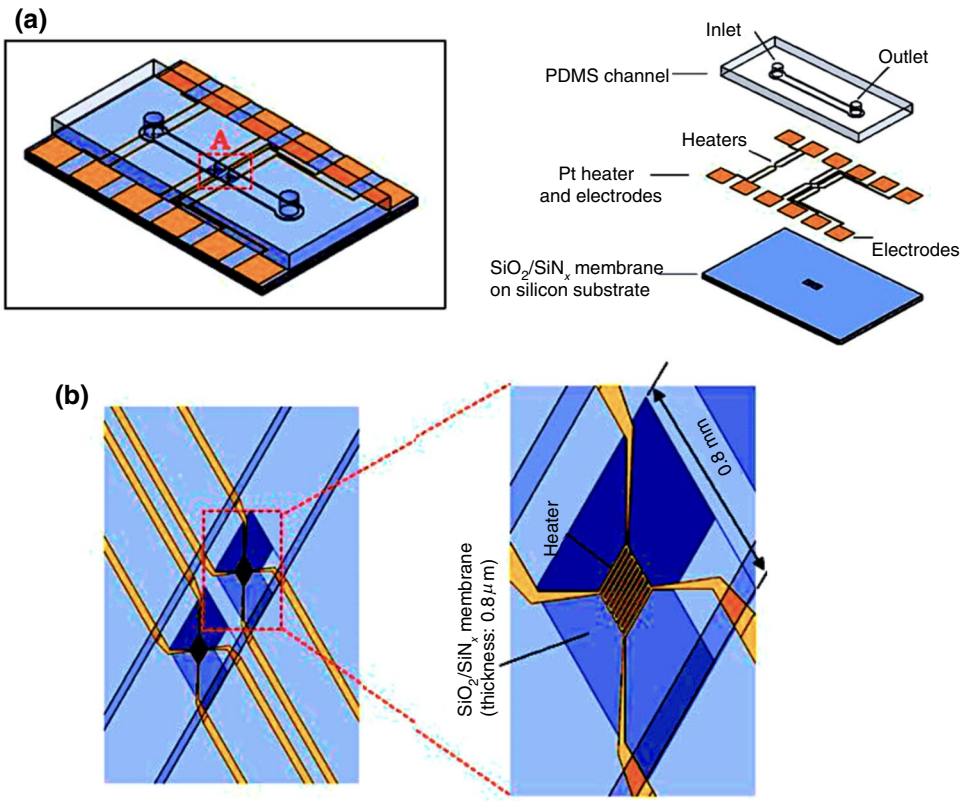

Fig. 1 The design and working process of the flowmeter

overall. The platform has an overall dimension of 11.5 mm in width, 17.5 mm in height, and 1.5 mm in depth.

Material selection

The best material to use to create adaptable fluidic and heat flux devices is thermoplastics. Their benefits over say different metals include their physical strength-to-mass ratio, corrosion immunity, stretch ability, the simplicity with which an almost infinite range of complicated forms and shapes may be created, and their complete recyclability. Their employment in heat exchange and thermal managing systems, nonetheless, may be compromised by their comparatively poor heat capacity and melting temperatures.

The following parameters were used to determine which synthetic polymers would be best for creating fluidic gadgets: the following requirements must be met: (1) physical flexibility; (2) chemical compliance with a variety of fluids, including freshwater, silicone lubricants, acidic and alkaline solutions, and coolants; (3) maximum continual service temperatures of 120 °C; and (4) abrasive resistance [23]. Polyethene was chosen as a suitable material for the aforementioned requirements. Black polymer strips with the channels of the microfluidic devices cut out of them were then placed between two translucent polypropylene sheets, which were joined to the black sheet by selective transfer welding processes.

Laser cutting

The polypropylene strips were cut into the forms necessary to construct the different "fluid and heat flux devices" using an LS1290 PRO CO_2 laser engraver with a maximal output of 80 W. Numerous factors, including cutting force, cutting edge hardness, slag, and the breadth of the heat impacted zone, influence cutting quality. The kerf breadth, which must be as tiny as feasible, is the most important variable.

Trial and error was used to find the cutting settings. Specifically, the chopping head velocity was 20 mm s^{-1}, the stand-off range was 0.5 mm, and the laser energy was kept at 90% of the maximum output (72 W). Machining was done repeatedly during engraving, eliminating around 0.1 mm of substance each time, to increase the cutting-edge polish. After slicing, abrasive material was employed to polish the surface and clean out any dust, slag, or debris from the edge of the plastic that might have impacted the quality of the weld.

Fabrication process

A silicon wafer with a diameter of 6 inches and a thickness of 500 µm was used to begin manufacturing. The P-type, (100)-oriented, 6-inch silicon wafer had 500 µm of thickness and was 500 µm wide. Firstly, silicon chip sheets of SiO_2 and SiN_x (300 nm of SiOz and 150 nm of SiN) were created by low-pressure chemistry vapor deposits (LPCVD) at temperatures of 600 °C for SiO and > 700 °C for SiN_x correspondingly [24].After that, 20-nm/200-nm-thick films of titanium (Ti)/Pt were formed (by hydrothermal method) and shaped using lift-off and standard photolithography. To provide galvanic isolation for the warmers, a second SiOz film (350 m thick) was formed by plasma-enhanced chemistry vapour device (PECVD) and structured. To prevent damaging impacts on the metallic surface at warm altitudes (750 °C) during the LPCVD procedure, the SiO_2 layers were formed during the PECVD procedure at a low heat (150 °C).

The fabrication process of the flowmeter is denoted in Fig. 2. The silicon metal (a), the SiO_2/SiN_2 layer (b), Ti/Pt layer (c), PECVD layer (d), etched wafer (e), coated wafer (f) and final flowmeter (g) are shown in different figures. Then, to provide a channel for the extensive etching procedure of the silicon wafer, the reverse SiO_2/SiN_x was etched. Shallow reactive-ion etching was used after a silicon profound etching to produce a mucosal coating. Using a slicing saw, the completed wafers were then cut into unit components.

The conduit was created using SU-8 negative lithography and a PDMS micromoulding process. In a nutshell, using a traditional photoresist, SU-8 with a 100 mm thickness m was printed onto the 4-inch silicon chip and utilized as a mould. The next step was to create PDMS by combining a base and hardener in 10:1 mass ratios. PDMS was put into the mould and dried on the hot plate (100 C for 15 min.) after refluxing the solution in a vacuum chamber for 10 min. Following oxygen laser irradiation, the PDMS down a part was subsequently attached to the unit gadget.

Thermal flowmeter characterization setup

The water flow was produced by external air density acting on the water tank. The flow rate was managed with a mass flow controller (MFC) called a Bronkhorst micro-Cori-flow M120. Water is flowing evenly from the MFC via the flowmeter and onto the scale mechanism. To prevent liquid from evaporating while the measurements were being taken, an evaporating trap was put on the collection glasses. Fluorinated ethylene polypropylene (FEP) tubing was used to link every component of the system. At the scales, the piping was attached to the needles. To prevent droplet development and enable a continuous measuring of the flow rate as time passed, the tip of the needles was submerged in the liquid in the gathering glass container.

The setup connection for flowmeter-based temperature compensation and measurement of the microfluidics is shown in Fig. 3. The block has a flow generation part, and reference flow measurement modules are used to measure and compensate the temperature of microfluidics. For

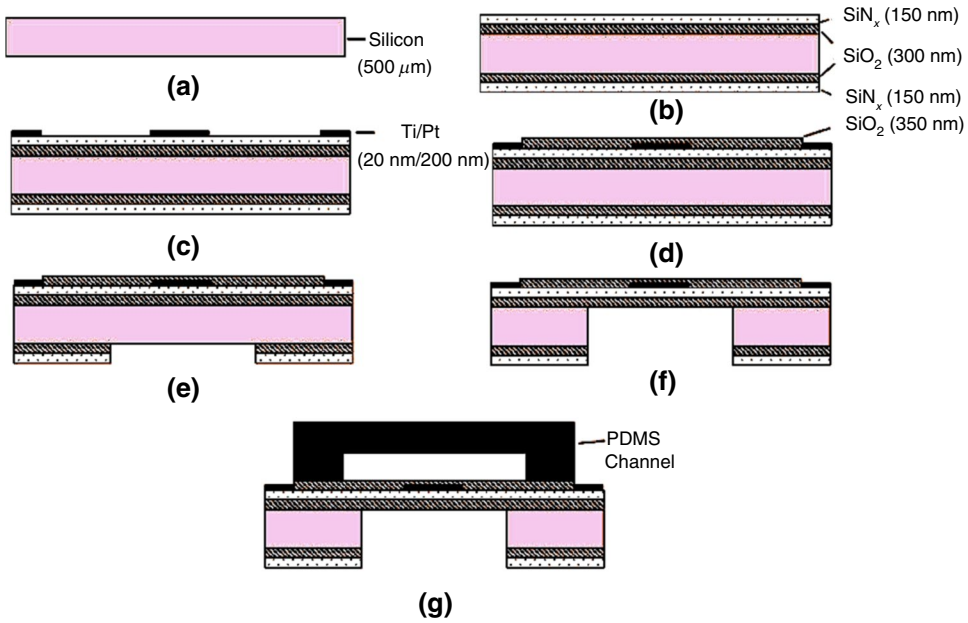

Fig. 2 The fabrication process of the flowmeter

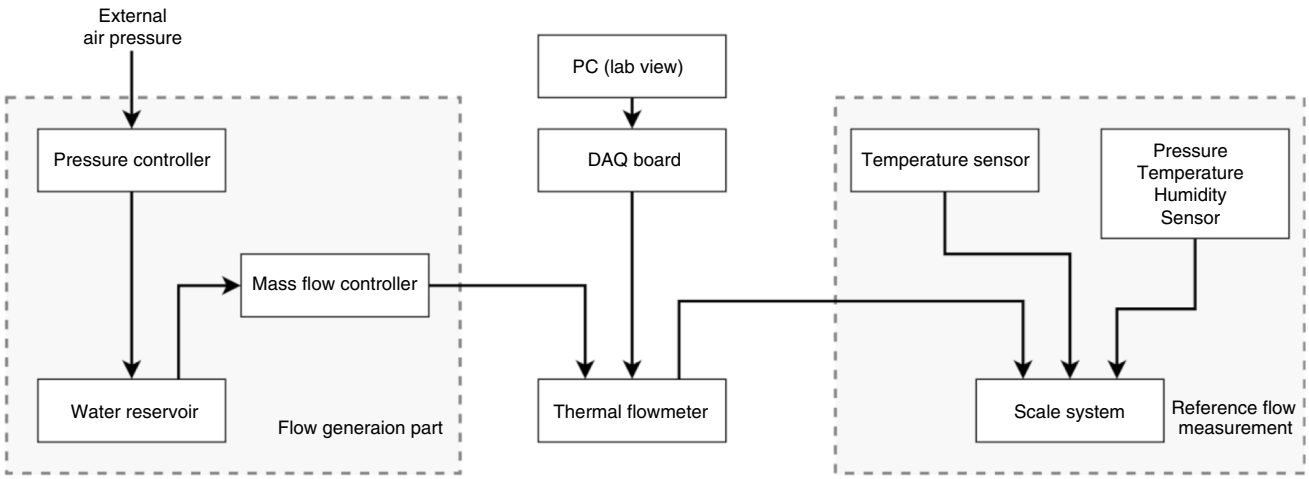

Fig. 3 The setup connection for flowmeter-based temperature compensation and measurement

the flow measuring characterization, four heater terminals on the flowmeter were electronically linked to a source measurement device. The supplied current was managed by a customized LabVIEW application, which also kept track of the flowmeter's electrical output. The temperature across the radiator was taken to determine heater impedance, and the electrical flow for CP mode was set at 3 mA. While the current flowing was beneficial for getting good sensitivity, there was a higher chance of bubble production owing to warming, particularly at a lower flow rate. Nevertheless, in CT mode, incoming power was detected and a closed-loop feedback mechanism regulated the flow to keep the impedance 3 greater than the impedance at room temperature.

Chip design and sensor installation

The temperature-dependent PCR chip is used to validate the physical structure before carrying out the numerical optimizing research. Here, the research describes a design for an S-shaped microchannel that includes two inlets for two flows of reagent introduction. The microchannel is made up of a 100-m-wide by 30-m-deep rectangle-shaped cross-section tube with an S-shaped unit in the middle that helps the reagent mix more uniformly. Well before exit,

there is a circle observation area on the linear microchannel, and there is just one outflow upstream for subsequent processing.

The glass slide is given a 20-min soak in acetone, followed by 15-s rinses in rubbing alcohol and DI freshwater, and final air-drying. After being plasma treated by a plasma generator, the previously described PDMS block adheres to a glass plate. Four phases make up the plasma therapy and bonding process: a. Insert a glass slide that has been polished and a PDMS block with the side of the channel visible into the plasma binding device. b. Vacuum the apparatus to a value of roughly 100 Kpa of tension.

c. Start a 40-s plasma live electrical explosion. d. Remove the PDMS blocks and quickly bind them to the microscope slide to prevent surface conformational changes or contamination (Fig. 4).

Temperature calibration and solution delivery

The microfluidic device is heated using a translucent toughened glass warmer and has a temperature inaccuracy of 0.1 °C. The impedance temperature heat controller is glued into the through-hole of the PDMS block and contains molten material to monitor the heat of the glassy slide's top part and store the information. To monitor and store the temperature readings of the convection cells, a high-precision thermostatic thermal sensor is placed inside the microchannels. The thermal link between the two discussed above is then taken into account when creating a compensating function. The functional computation indicates that it is possible to describe the temperatures of the microfluid

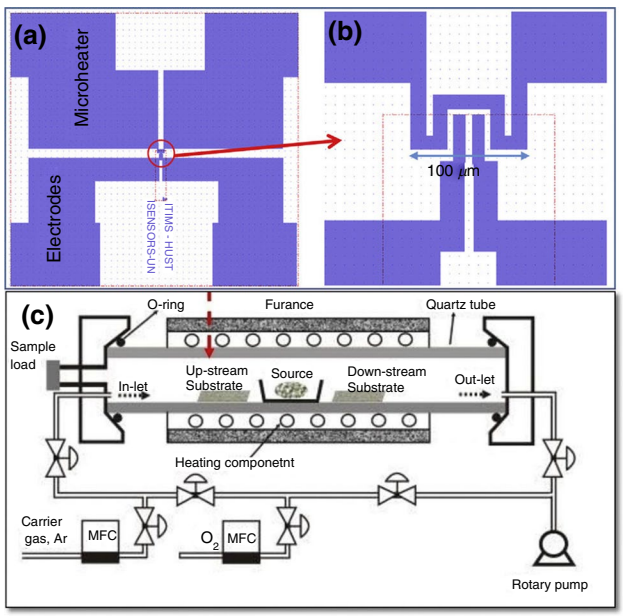

Fig. 4 Chips and design

without using precision heating sensors by measuring the heat of the glass plate.

A PCR amplification research that was extremely temperature-sensitive is provided to evaluate the effectiveness of measuring temperature. Thus, a flow pattern is created at the very start of the chip by pumping two streams of water solution via the inlets with distinct, separately regulated programmed flow controllers. The S-shaped tube is then filled with laminar fluids to provide better reagent interaction. The heater is precisely calibrated to a predetermined heat and runs for 20 min once the fluid has filled the platform. Then use a microscope to study the fluorescence impact in the region upstream of the microchannels.

Numerical analyses

The numerical analysis setup and the parameters are discussed in the following subsection.

Control equation and boundary condition settings

For modelling, the mechanical field components of the occurrences and solids and liquids heat exchange are employed.

Assuming that all heat transmission between solids and liquids occurs in this way, the energy-saving expression is shown in Eq. (2).

$$\rho \times V \times C_{\mathrm{p}} \times \frac{\mathrm{d}T}{\mathrm{d}t} + \nabla(-V \times k \times \nabla T) = Q_{\mathrm{o}} \tag{2}$$

where k is the thermal conductance, V is the area of the warmed item, C_{p} is the capacitor evaluated at steady pressures, and Q_{o} is the rate at which energy is produced across the whole system. Material intensity is denoted ρ.

A steady energy P_{o} and a status indication StateHeater (specified in the Event interfaces) are chosen as thermal power sources to replicate the heater's heat regulation, and the electricity creation rate is adjusted using Eq. (3).

$$Q_{\mathrm{o}} = P_{\mathrm{o}} \times S_{\mathrm{h}} \tag{3}$$

S_{h} denoted the state heater, and the steady energy is indicated P_{o}. Given that thermal protection is expected to cover the heater's bottom, the boundary requirement is specified using Eq. (4).

$$n(-k \times \nabla T) = h_{\mathrm{c}}(T - T_{\mathrm{o}}) \tag{4}$$

T_{o} is the outside temperatures and h_{c} is the heat flow ratio for natural circulation. The plank/s constant is denoted k, the present temperature is denoted T, and the temperature deviation is denoted ∇T. The system's radiative heat flow to the environment can be adjusted using Eq. (5).

$$n(-k \times \nabla T) = \tau\rho\left(T^{k} - T_{o}^{k}\right); \quad \text{where } k = 4 \tag{5}$$

The temperature of the microfluidics is denoted T, the channel length is denoted n, and the deviation is denoted ∇T. τ denotes the material's transmittance, $0 < \rho < 1$, and σ denotes the Stefan–Boltzmann constants. Among the heating mantle and the glass slides, there is interface heat loss that mostly consists of contacting and spacing heat capacity, which is represented in Eq. (6).

$$n(-k \times \nabla T) = h\left(T_{d} - T_{u}\right) + \frac{rQ_{o}}{A_{d}} \tag{6}$$

The temperature capacity is denoted T_d, the compensated temperature is denoted T_d, and r is the heat partition coefficient. The generated energy is denoted Q_o, the gain is denoted A_d, and the heat coefficient is denoted h. the heat coefficient is indicated in Eq. (7).

$$h = h_{c} + h_{g} \tag{7}$$

The contact and gap heat are expressed h_c and h_g. The surface smoothness, microhardness, and contacting pressure of the substance are all strongly correlated with the heat transport ratio of heat transfer impedance. The contact heat of the flowmeter is denoted in Eq. (8).

$$h_{c} = 1.25k \times \frac{m_{a}}{\propto_{a}}\left(P/H_{c}\right)^{0.85} \tag{8}$$

where the asperities mean slopes and elevation surface smoothness are, correspondingly, m_a and $\propto_a$ is the heat conductance of the substances in interaction. P is the contact force between the glass sliding and the burner. The glass's hardness value is H_c. The gap heat is constant and the value is fixed for the experimental analysis.

The kind of gas and contact temperature among two touching objects affect the separation heat impedance. Although the value range may be tested, there is currently no dedicated expression method.

Parameter settings in the simulation

Here, the research did not suggest a real 3D model to compute the heat transfer procedure because the 3D model's architecture is quite regular and has comparable abutments. The research has provided a 2D numerical model of a transverse cross contour for clarity. COMSOL Multiphysics 5.4, a piece of finite element technology, is used to run the thermal transfer simulation. A discontinuous grid for the simulation study, several domains and border elements in various element widths, and grid-independent testing are all provided in the Supplementary Materials along with convergence solution techniques.

This section discusses the design and working principle of the flowmeter to compensate for and measure the temperature of microfluidics in drug injection applications. The mathematical model helps to produce results with higher accuracy.

Results and discussion

Platinum (Pt) impedance sensors use contact conductivity and energy to monitor temperature signals. The ability of ambient materials put close to the detector to transmit heat has a big impact on how response signals are picked up. The Pt sensor is first placed directly into the hole, brought as near to making touch with the surface of the glassy slides as feasible, and then sealed with gel, for example setting the goal temperatures to 60 C and having the hole's diameter twice as large as the sensor's. The 2D microfluidic microchip heat exchange system's thermal variation is depicted numerically.

The glass surface temperature analysis of the proposed MFTCTM is shown in Fig. 5. The simulation analysis is done by varying the test temperature from 30 to 100 °C, and the respective glass surface temperature of the flowmeter is then analysed and measured. The microfluidic temperature and the glass surface temperature are directly related to each other. The glass surface temperature increases when the microfluidic temperature rises above some threshold value. The mechanically pulsating heat exchanger compensates for the heat and thus helps in drug injection applications to reduce body heat using microfluidics.

The glass surface temperature analysis under the microfluidics condition is analysed, and the results are plotted in Fig. 6. The variation in the temperature of the microfluidics concerning the body temperature is computed, and the

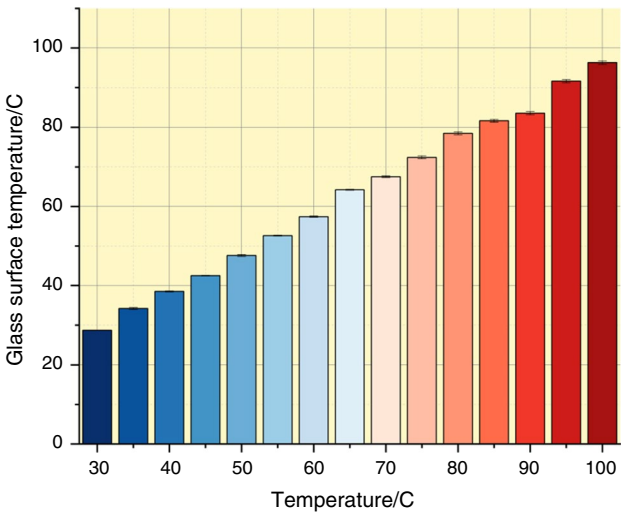

Fig. 5 Glass surface temperature analysis

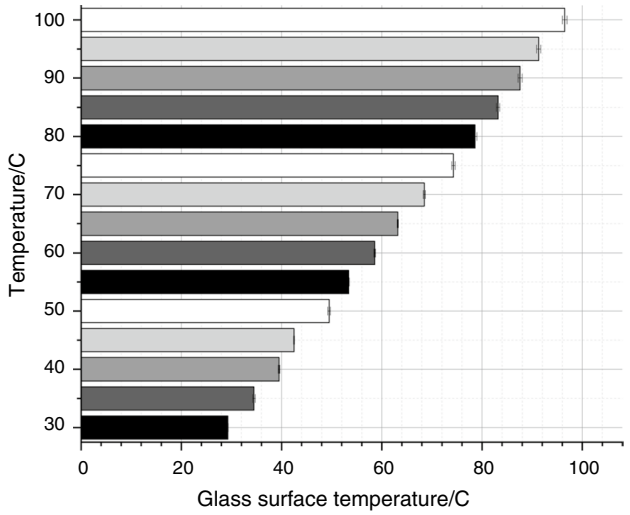

Fig. 6 Glass surface temperature analysis under the microfluidics condition

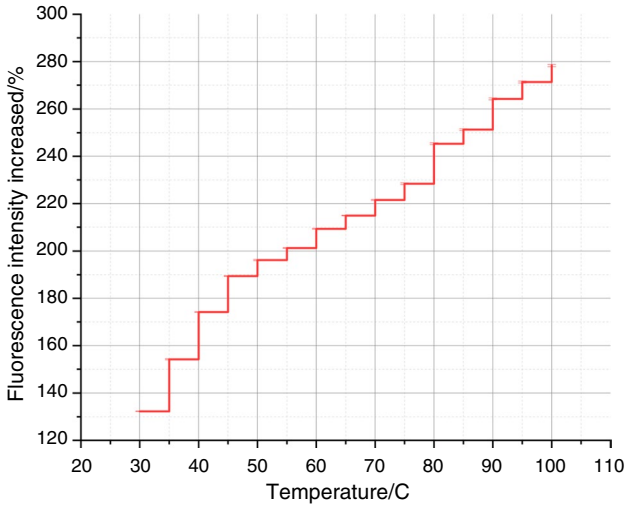

Fig. 7 The increased fluorescence intensity analysis

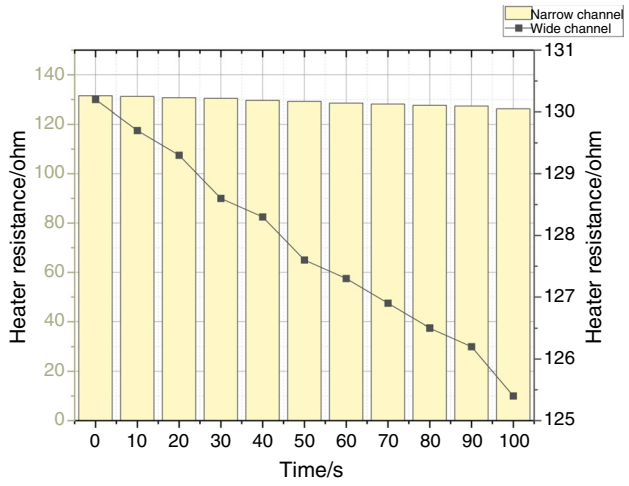

Fig. 8 Heater resistance analysis of the proposed system

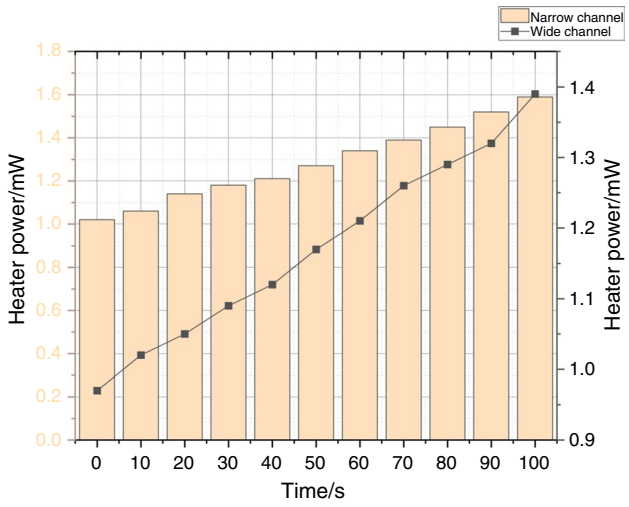

Fig. 9 Heater power analysis of the mechanically pulsating heat exchanger

results show a linear relationship between those temperatures. The designed mechanically pulsating heat exchanger compensates for body temperature and helps reduce the microfluidics temperature in drug injection applications. The results show that the MFTCTM is the most accurate way to measure and adjust the temperatures in microfluidic systems.

In Fig. 7, the increased fluorescence intensity analysis of microfluidics concerning temperature is analysed and plotted. As the microfluidics temperature increases, the fluorescence intensity in the flowmeter increases, which results in the highest compensation. The MFTCTM shows the highest detection because of the optimum structure of the flowmeter and the materials used for its construction. The intensity results are analysed from 30 to 100 °C with a step count of 10 °C, which ensures the performance of the mechanically pulsating heat exchanger in all the temperature variations.

The mechanically pulsating heat exchanger performance is analysed in microfluidics, and the results are plotted in Fig. 8. The analysis is done by varying the channel width in two conditions, such as a narrow channel and a wide channel. The heater's resistance to temperature is directly related to the channel width. The narrow channel has lower resistance, whereas the wider channel has higher resistance. The heater resistance is analysed concerning the timing variations. As time goes on, the resistance of both narrow and wide channels also reduces.

The heater power is calculated for the mechanically pulsating heat exchanger, and Fig. 9 displays the findings

Table 1 Flow rate analysis of the mechanically pulsating heat exchanger-based flowmeter

Flow rate/g h^{-1}	Heater resistance/ohm		Heater power/mW	
	Narrow channel	Wide channel	Narrow channel	Wide channel
0.5	131.5	131.1	1.1	0.7
1	130.4	130.4	1.6	1.2
1.5	130.1	129.7	2.1	1.4
2	129.8	129.2	2.4	1.6
2.5	129.7	128.2	2.7	1.8
3	129.3	127.5	3.1	1.9

about time variation. The respective power provided by the mechanically pulsating heat exchanger grows as time passes. In the study, both the narrow channel and the large channel are evaluated. The findings indicate that the narrow channel functions effectively and generates more energy than the broad channel. The outcomes are further improved by the choice of materials and production methods.

The results of the flow rate analysis of the mechanically pulsating heat exchanger-based flowmeter to detect and correct the microfluidics temperature are displayed in Table 1 for various conditions. The heat resistance and heater power for various flow rates are analysed, and the results are summarized. The findings guarantee the rice in terms of heater resistance and heater power about the increase in flow rate. Utilizing a mechanically pulsating heat exchanger, the suggested system achieves more accurate temperature monitoring and adjustment in microfluidics.

Conclusions

Micromachining is used to develop and construct a MEMS flowmeter with a microfluidic tunnel to monitor low flow rates for infusion-pump validation. A silicon substrate, a Pt heating film atop a SiO/SiN small membrane, and a PDMS mould with dimensions of 11.5 mm (widths) and 17.5 mm (lengths) 3 mm made up the MEMS flowmeter (heights). The flowmeter's efficiency is assessed using the conventional GM in two distinct modes (the CP and CT variants) and 2 distinct channel lengths (0.5 mm and 1.5 mm). In the 0.5–2.5 g h^{-1} range, the measurement system in CT function with a 0.5-mm-wide channel exhibits the best efficiency, with an inaccuracy that is five times lower than that of conventional portable infusing pumps. To examine the interaction between the glass substrates of a conventional microfluidic system and the microfluidics, a heat exchange simulation was provided using a mechanically pulsating heat exchanger. The millimetre-scale commercial heating element might be used for temperature detection of microscale liquids thanks to an intelligent building system and fluid metals. The technique gets over the problems with thermal monitoring for microfluidics. From 30 to 100 °C, the linear trend spectrum of observed temperature is shown, and the uncertainty error is less than 0.5 °C. The thermal precision of this technique has also been clarified by temperature-sensitive amplification tests using nucleic acids. Consequently, it can be inferred that this technique has great promise for micro–macro-interaction detection and is useful for purposes beyond microfluidic ones. Microfluidic devices offer an appropriate regulated environment for cell cultivation and drug testing on a broad range of cells, like cancer, liver, and microbial. The regulated atmosphere permits the observation of cell cultures over lengthy periods of time. Thermal resistance is a measure of heat flow resistance across a certain thickness of material. Thermal resistance is calculated by dividing a sample's thickness by its thermal conductivity. Electrical resistance, or resistance to electricity, is a force that opposes the passage of current. In this manner, it indicates the challenge it is for current to flow. Resistance values are measured in ohms.

Acknowledgements Magda Abd El-Rahman extends their appreciation to the Deanship of Scientific Research at King Khalid University, Abha, Saudi Arabia, for funding this work through Large Groups Project under grant number RGP 2/69/44.

References

1. Alizadeh A, Movahedi P, Mirzahosseini S, Ekhtiari S. Investigating different types of fluids in pulsating heat pipes for improving heat transfer in an air-cooled heat exchanger. Proc Inst Mech Eng Part A J Power Energy. 2022. https://doi.org/10.1177/09576509221076 6.
2. Grimstein M, Yang Y, Zhang X, Grillo J, Huang SM, Zineh I, Wang Y. Physiologically based pharmacokinetic modelling in regulatory science: an update from the US Food and Drug Administration's Office of Clinical Pharmacology. J Pharm Sci. 2019;108(1):21–5.
3. Abu-Hamdeh NH, Bantan RA, Aalizadeh F, Alimoradi A. Controlled drug delivery using the magnetic nanoparticles in non-Newtonian blood vessels. Alex Eng J. 2020;59(6):4049–62.
4. Parot J, Caputo F, Mehn D, Hackley VA, Calzolai L. Physical characterization of liposomal drug formulations using multi-detector asymmetrical-flow field flow fractionation. J Control Release. 2020;320:495–510.
5. Doh I, Sim D, Kim SS. Microfluidic thermal flowmeters for drug injection monitoring. Sensors. 2022;22(9):3151.
6. Bhavana HT, Sunil MA, Sanjana T, Harshitha B. Recent Advances in Drug Delivery Systems: MEMS Perspective. In: Disruptive developments in biomedical applications, 1st edition, Chapter 20, pp 299–309 (2023).
7. Meng J, Yu C, Li S, Wei C, Dai S, Li H, Li J. Microfluidics temperature compensating and monitoring based on liquid metal heat transfer. Micromachines. 2022;13(5):792.

8. Zhao PJ, Gan R, Huang L. A microfluidic flow meter with micromachined thermal sensing elements. Rev Sci Instrum. 2020;91(10):105006.
9. Jderu A, Soto MA, Enachescu M, Ziegler D. Liquid flow meter by fibre-optic sensing of heat propagation. Sensors. 2021;21(2):355.
10. Van Erp R, Soleimanzadeh R, Nela L, Kampitsis G, Matioli E. Co-designing electronics with microfluidics for more sustainable cooling. Nature. 2020;585(7824):211–6.
11. Chen G, Zheng J, Liu L, Xu L. Application of microfluidics in wearable devices. Small Methods. 2019;3(12):1900688.
12. Zhao X, Gao W, Yin J, Fan W, Wang Z, Hu K, Mai Y, Luan A, Xu B, Jin Q. A high-precision thermometry microfluidic chip for real-time monitoring of the physiological process of live tumour cells. Talanta. 2021;226:122101.
13. Saad MG, Selahi A, Zoromba MS, Mekki L, El-Bana M, Dosoky NS, Nobles D, Shafik HM. A droplet-based gradient is microfluidic to monitor and evaluate the growth of Chlorella Vulgaris under different levels of nitrogen and temperatures. Algal Res. 2019;44:101657.
14. Kong M, Li Z, Wu J, Hu J, Sheng Y, Wu D, Lin Y, Li M, Wang X, Wang S. A wearable microfluidic device for rapid detection of HIV-1 DNA using recombinase polymerase amplification. Talanta. 2019;205:120155.
15. Coluccio ML, Perozziello G, Malara N, Parrotta E, Zhang P, Gentile F, Limongi T, Raj PM, Cuda G, Candeloro P, Di Fabrizio E. Microfluidic platforms for cell cultures and investigations. Microelectron Eng. 2019;208:14–28.
16. Zhu JY, Suarez SA, Thurgood P, Nguyen N, Mohammed M, Abdelwahab H, Needham S, Pirogova E, Ghorbani K, Baratchi S, Khoshmanesh K. Reconfigurable, self-sufficient convective heat exchanger for temperature control of microfluidic systems. Anal Chem. 2019;91(24):15784–90.
17. Bunge F, van den Driesche S, Waespy M, Radtke A, Belge G, Kelm S, Waite AM, Mirastschijski U, Vellekoop MJ. The microfluidic oxygen sensor system is a tool to monitor the metabolism of mammalian cells. Sens Actuators B Chem. 2019;289:24–31.
18. Peng J, Fang C, Ren S, Pan J, Jia Y, Shu Z, Gao D. Development of a microfluidic device with precise on-chip temperature control by integrated cooling and heating components for single cell-based analysis. Int J Heat Mass Transf. 2019;130:660–7.
19. Luo X, Su P, Zhang W, Raston CL. Microfluidic devices in fabricating nano or micromaterials for biomedical applications. Adv Mater Technol. 2019;4(12):1900488.
20. Abdel-Latif K, Epps RW, Kerr CB, Papa CM, Castellano FN, Abolhasani M. Facile room-temperature anion exchange reactions of inorganic perovskite quantum dots enabled by a modular microfluidic platform. Adv Func Mater. 2019;29(23):1900712.
21. Arqub OA, Abo-Hammour Z. Numerical solution of systems of second-order boundary value problems using continuous genetic algorithm. Inf Sci. 2014;279:396–415.
22. Abo-Hammour Z, Abu Arqub O, Momani S, Shawagfeh N. Optimization solution of Troesch's and Bratu's problems of ordinary type using novel continuous genetic algorithm. Discrete Dyn Nat Soc. 2014:401696
23. Zahran EH, Arqub OA, Bekir A, Abukhaled M. New diverse types of soliton solutions to the Radhakrishnan–Kundu–Lakshmanan equation. AIMS Math. 2023;8:8985–9008.
24. Cavaniol C, Cesar W, Descroix S, Viovy JL. Flowmetering for microfluidics. Lab Chip. 2022;22(19):3603–17.
25. Cooksey GA, Patrone PN, Hands JR, Meek SE, Kearsley AJ. Dynamic measurement of nanoflows: realization of an optofluidic flow meter to the nanoliter-per-minute scale. Anal Chem. 2019;91(16):10713–22.
26. Wu T, Shen J, Li Z, Xing F, Xin W, Wang Z, Liu G, Han X, Man Z, Fu S. Microfluidic-integrated graphene optical sensors for real-time and ultra-low flow velocity detection. Appl Surf Sci. 2021;539:148232.
27. Cao Y, Wang T, Sepúlveda N. Microfluidic thermal flow sensor based on phase-change material with ultra-high thermal sensitivity. J Mater Chem C. 2023;11 (4)1278–84.